Journal of Power Sources 564 (2023) 232817

Contents lists available at ScienceDirect

Journal of Power Sources

journal homepage: www.elsevier.com/locate/jpowsour

DFT calculation, a practical tool to predict the electrochemical behaviour of organic electrolytes in aqueous redox flow batteries

Juan Asenjo-Pascual [a,b,**], Ivan Salmeron-Sanchez [a], Pablo Mauleón [b,c], Maddalen Agirre [d], Ana Catarina Lopes [d,e,f], Oihane Zugazua [d], Eduardo Sánchez-Díez [d,*], Juan Ramón Avilés-Moreno [a], Pilar Ocón [a]

[a] Department of Applied Physical Chemistry, Universidad Autónoma de Madrid, Spain
[b] Department of Organic Chemistry, Universidad Autónoma de Madrid, Spain
[c] Institute for Advanced Research in Chemical Sciences (IAdChem), Universidad Autónoma de Madrid, c/Fco. Tomás y Valiente 7, 28049, Cantoblanco, Madrid, Spain
[d] Centre for Cooperative Research on Alternative Energies (CIC EnergiGUNE), Basque Research and Technology Alliance (BRTA), Alava Technology Park, Albert Einstein 48, 01510, Vitoria-Gasteiz, Spain
[e] IKERBASQUE, Basque Foundation for Science, Plaza Euskadi 5, 48009, Bilbao, Spain
[f] Macromolecular Chemistry Group (LABQUIMAC), Department of Physical Chemistry, Faculty of Science and Technology, University of the Basque Country, UPV/EHU, Barrio Sarriena, s/n, 48940, Leioa, Spain

HIGHLIGHTS

- 2,2′-Bipyridinium salts have been selected as negolytes for this study.
- DFT calculation let correlate structural parameters with different redox properties.
- NBO and ADCH charges shed light on the stability of reduced species.
- Double capacity retention of selected negolyte shows the predicting ability of DFT.

GRAPHICAL ABSTRACT

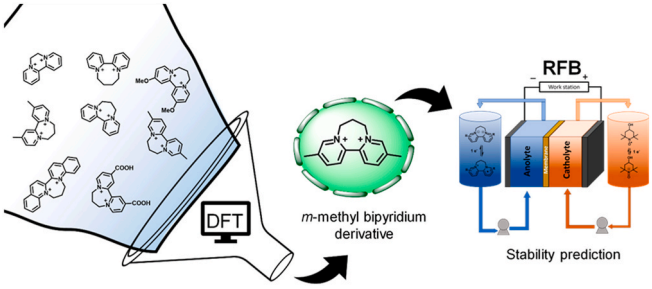

ARTICLE INFO

Keywords:
Aqueous organic redox flow batteries
DFT calculations
NBO delocalization
ADCH charge Analysis
Bipyridine negolytes

ABSTRACT

Herein, a computational predictive tool for redox flow batteries based on NBO and ADCH charge distribution studies is presented and supported by experimental evidence. Using highly water soluble (>2 M) non-planar 2,2′-bipyridinium salts as a case of study, this work presents a DFT protocol that successfully predicts the stability and forecasts their potential application as active materials for Aqueous Organic Redox Flow Batteries (AORFB). An initial theoretical-experimental characterization of selected bipyridines served to determine the effect of the ring size, geometry, and electron density on the physico-chemical properties of the materials. Nonetheless, the NBO and ADCH charge analyses were essential tools to understand the stability of the reduced species in terms of electronic delocalization and the importance of the molecular design on the stability of electrolyte for AORFB. Based on these results, the cell performance of seven-membered 2,2′-bypiridinium salt, (**2**), and *m*-Me substituted

* Corresponding author. Centre for Cooperative Research on Alternative Energies (CIC EnergiGUNE), Basque Research and Technology Alliance (BRTA), Alava Technology Park, Albert Einstein 48, 01510, Vitoria-Gasteiz, Spain.
** Corresponding author. Department of Applied Physical Chemistry, Universidad Autónoma de Madrid, Spain.
E-mail addresses: juan.asenjo@uam.es (J. Asenjo-Pascual), esanchez@cicenergigune.com (E. Sánchez-Díez).

https://doi.org/10.1016/j.jpowsour.2023.232817
Received 14 October 2022; Received in revised form 26 December 2022; Accepted 11 February 2023
Available online 25 February 2023

homologous, (**4**), were compared. The significantly lower capacity decay rendered by compound **4** based electrolyte, (0.35%/cycle) compared with compound **2** based electrolyte, (0.71%/cycle) was in good agreement with the predicted stability. The aim of this work is to highlight the powerful synergy between DFT calculations and organic chemistry in predicting the behaviour of different negolytes.

1. Introduction

Intermittency is the main limitation towards the deployment of renewable energy to confront climate change and empower decarbonisation plans [1] where electrochemical energy storage will be crucial for the energy transition. However, installation and maintenance costs still prevent storage from penetrating the grid [2]. Long-life-low-cost batteries are needed to fulfil Strategic Energy Technology Plan targets for stationary energy storage, which have been defined in terms of cost and durability as 0.05 € kWh^{-1} $cycle^{-1}$ for over 10.000 cycles [3].

In this context, Redox Flow Batteries (RFB) have emerged as suitable candidates due to their architecture and unique capability to decouple energy and power [4]. Although all-vanadium RFB stand as the state of the art and have reached commercial fruition [5], they still present significant limitations: mainly related to the limited availability of V_2O_5, which is the raw material required for the preparation of vanadium electrolytes. Organic electrolytes based on earth abundant elements have been proposed as a cost-efficient and green alternative to overcome these limitations. Those can be produced in large-scale at will and potential low cost, and in addition, they exhibit a high tunability of their properties [6,7]. In principle, solubility, redox potential, and stability of the active materials could be modulated to produce a battery with higher energy density, higher cell-voltage, and better long-term performance. Concerning the active materials design, chemistry offers numerous combinations which could be obtained following organic chemistry guidelines. Along these lines, computational tools provide strong support to screen this vast chemical space. Indeed, Density Functional Theory (DFT) calculations have been applied in the characterization of the electronic and structural parameters of different compounds attempting to predict their behaviour in a RFB [8].

Among the variety of molecules that have been proposed as negolytes for AORFB, viologen derivatives have attracted increased interest on account of their interesting properties: low-cost, based on a direct synthesis from bipyridines, high-water solubility (1–2 M), fast electrokinetics (>10^{-3} cm^2/s), and negative redox potential (~−0.4 V). Significant advances have been made on the achievement of stable 4,4′-bipyridinium compounds by applying molecular engineering principles, which have ultimately leaded to one of the highest capacity retentions reported to the date [9]. Dealkylation and dimerization, which were appointed as main degradation mechanism responsible for the capacity fade, have been partially addressed [10]. In this context, computational studies have been devoted to better understand the relevance of the structure distortions and electronic characteristics on the electrochemical properties of the active materials [11]. In particular, some authors have envisioned a direct correlation between the stability of the reduced form and the delocalization of the radical electron across the bipyridyl core in 2,2′ bipyridinium salts [12]. Huang et al. have synthesized and electrochemically characterized different diquat derivatives and concluded that π-conjugation in highly planar structures plays a pivotal role on the reversibility of the redox process and the cycling stability of the compound [13].

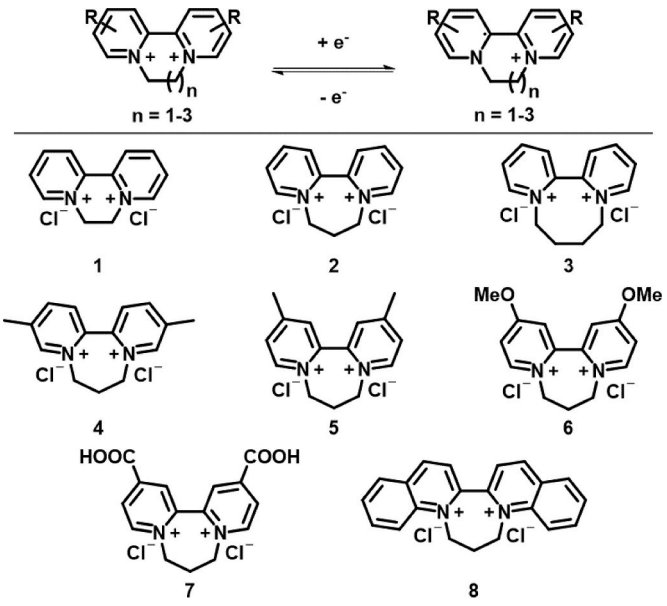

Fig. 1. Schematic redox reaction (top) and the eight redox active materials prepared in this work.

Despite these advances, the durability of AORFB reported to date [14] is rather low for a technology that is meant to provide solutions for the next 20 years; this lack of stability is more evident in high energy density systems, that report capacity losses close to 1% per day [10,15]. Capacity fade is typically a consequence of the decomposition of the active materials, notwithstanding, only few recent studies have been focused on the stability and behaviour of charged species [16]. While experimental and theoretical studies put special emphasis on fundamental properties such as redox potentials, kinetic constants, diffusion coefficients and reversibility of the redox process, there is a lack of much needed studies on the evaluation and understanding of the chemical stability of active materials.

The present work represents an expansion of the use of DFT calculation in RFB to gain insights on the stability of charged species. Herein, several 2,2′-bipyridinium salts have been selected to study the effect that structural and electronic characteristics exert on the performance of organic redox active materials. Considering the smaller contribution of the planar π-conjugation to the stability in the 7-membered bipyridinium compounds, 1,1′-1,3-propylene-2,2′-bipyridinium derivatives were chosen for evaluating the stabilization promoted by substituents on the pyridinium rings. Importantly, detailed evaluation of the electrochemical properties and charge distribution by NBO and ADCH analyses allow to predict the stability of these compounds. This prediction could be confirmed experimentally when bipyridinium salts **2** and **4** (see Fig. 1) were paired with TEMPOL as posolyte for chemical stability evaluation. The higher charge delocalization on the reduced bipyridinium salt **4** predicted by DFT calculations turned into lower capacity decay over time (0.285 mAh/cycle, 0.71%/cycle vs 0.141 mAh/cycle, 0.35%/cycle, compound **2** and **4** respectively), thus confirming the potential of computational tools in understanding the performance of redox active materials (RAM) in real applications.

2. Experimental

2.1. Chemicals and instrumentation

Unless otherwise noted, reagents and materials were purchased from commercial suppliers and used without further purification. Air sensitive reactions were conducted under inert atmosphere making use of previously dried argon gas. Rotary evaporator was used for the removal of solvents under reduced pressure. Purity of final compounds was assessed by ^1H NMR. Final materials were dried under vacuum prior to

be used.

Monodimensional and/or bidimensional Nuclear Magnetic Resonance (NMR) proton and carbon spectra were recorded at 300 MHz for ^{1}H NMR and 75.5 MHz for ^{13}C NMR at 25 °C on a 300 MHz spectrometer using dimethylsulfoxide-*d6* (DMSO-d_6) and D_2O as solvents and Me_4Si as internal standard. Chemical shifts (δ) are reported in ppm relative to residual solvent signals (dimethylsulfoxide-*d6* 2.50 ppm for ^{1}H NMR, 39.5 ppm for ^{13}C NMR; D_2O 4.79 ppm for ^{1}H NMR) and coupling constants (*J*) in hertz (Hz). The data are represented as follows: chemical shift (ppm), multiplicity (s = singlet, d = doublet, t = triplet, q = quartet, m = multiplet or unresolved, bs = broad signal) coupling constant(s) (*J*), integration. ^{13}C NMR spectra were recorded with ^{1}H decoupling.

2.2. Synthesis of 2,2′-bipyridines 1–8

2,2′-bipyridine derivatives were synthesized by introduction of alkyl substituents at *N,N′* atoms through a straightforward procedure either by regular (Method A) or microwave-assisted (Method B) heating in a solvent-free process. The corresponding derivatives were next subjected to anion exchange procedure using IRA-900 chloride form resin.

METHOD A: 2,2′-bipyridine derivatives were synthesized following already reported literature procedures[1]. A solution of 2,2′-bipyridine (1 Eq) in the corresponding dibromoalkane (2–23 Eq) was refluxed for 16 h, during which a precipitate accumulated. The reaction was cooled down to room temperature and the solid was filtered and washed with acetone and hexanes. The solid was then subjected to anion exchange procedure using IRA-900 chloride form resin and water was evaporated under reduced pressure on a rotary evaporator. The final compound was dried under vacuum to afford the desired 2,2-bipyridine.

METHOD B: To a microwave vial equipped with a magnetic bar (for microwave reactor), bipyridine (1 Eq), the corresponding dibromoalkane (1.3–4 Eq) and acetonitrile were added. The vial was sealed and placed in the microwave reactor. The appearance of a solid indicated the formation of the product. The solid was filtered and washed with acetonitrile to ensure the elimination of the dibromoalkane excess and was then subjected to anion exchange procedure using IRA-900 chloride form resin. Water was evaporated under reduced pressure on a rotary evaporator. Before characterization, the product was dried at 65 °C in the oven.

More information regarding the method and the exact amounts used as well as the ^{1}H and ^{13}C NMR spectra for each compound can be found in the Supporting Information (Figs. S1–16).

2.3. Electrochemical characterization

Glassy carbon (6.1204.300 from Metrohm, 3.0 mm diameter) was used as working electrode (WE), Pt electrode was used as counter electrode (CE) and Ag/AgCl as reference electrode (RE) in all the electrochemical measurements. RDE were conducted using a Metrohm Autolab Motor Controller. Both CV and RDE tests were performed using an Autolab electrochemical system II PGSTAT30 potentiostat. More information about the rotating disk electrode analysis for each compound can be found in the Supporting Information (Figs. S17–21).

2.4. Solubility

The solubilities of the different bipyridines were measured by UV–Vis spectroscopy. Calibration curves were obtained for all the compounds. An aliquot of the saturated solution of the corresponding bipyridine derivative was diluted until the absorption of the sample fits the corresponding calibration curve. By multiplying the concentration achieved from the sample interpolation by the corresponding dilution factor, the maximum solubility of the compounds was calculated. The calibration curves and the UV–Vis spectra can be found in the Supporting Information (Figs. S24–27).

2.5. DFT calculations

All the calculations were carried out using a Gaussian16 software package [17] at different DFT levels and the 6–311++G(d,p) basis set [18]. The most stable conformers of the redox species of each electrolyte were selected for further structural optimization and calculation of their relative energies (including ZPE corrections) and many other molecular and electrochemical parameters described below using three density functional approaches (B3LYP [19], M062X [20], and B97D3 [21] functionals) and the 6–311++G(d,p) basis set. The M062X functional is a high nonlocality approach with double amount of nonlocal exchange (2x), parametrized only for nonmetals and containing a treatment of noncovalent interactions. These three different DFT methods were compared to make certain the internal consistency of the theoretical models and their predictive values [22].

Comparison of the results obtained with different functionals is a challenging task due to the reproducibility of the results with other systems which are not always evident. In this way, we have tested the results with the B3LYP, M062X and B97D3 approaches. In this work, only the results achieved using B3LYP level have been shown.

Solvent effect (water, in this case) is considered using the IEF-PCM methodology [23] implemented in Gaussian16. From the IEF-PCM methodology results, it was found that the implicit solvent effects were negligible. The optimized structure as well as information about the geometric, Mulliken, Hirshfeld and ACDH charges and NBO analysis can be found in the Supporting Information.

2.6. Cell cycling

The flow cell was set up using two copper current collector plates, two composite bipolar plates (carbon-polyolefin), graphite felts electrodes (SGL GFD 4.6 EA), four sheets of gasket (flat, polyolefin) and FAA-3-50 membrane from Fumatech®. Membranes were soaked in 1 M of NaCl solution for 24 h prior to be used. 15 mL of a 0.1 M solution of corresponding bipyridine (2 or 4 respectively) in 1 M NaCl and 20 mL of a 0.15 M TEMPOL solution in 1 M NaCl were used as negolyte and posolyte respectively. The active area of the cell was 4 cm^2. A Watson-Marlow 323 peristaltic pump was used to circulate the electrolyte through the system at a flow rate of 40 mL/min. The reservoirs were purged with Argon (99.999%) for 30 min to remove the O_2 before cycling. The whole system was placed inside a homemade glovebox which was purged with Argon for 30 min. The cell was galvanostatically charged/discharged at room temperature using a Biologic multichannel potenciostatic-galvanostaic coupled to an impedance module BSC-815 in the voltage range of 0–1.57 V for the compound **2** and 0–1.67 V for the compound **4** at current density of 100 mA/cm^2. When the cutoff potentials were reached the cell was further charged/discharged applying a constant voltage as defined by the cut off limits until the current density decreased below 12.5 mA/cm^2. This method was applied to ensure that both experiments have reached the desired state of charge making the results comparable. Note that a potentionstatic electrochemical impedance spectroscopy (EIS) of both systems were measured before and after cycling, showing in all the cases similar resistance (≈2.5 Ω cm^2). The impedance before and after cycling as well as the evolution of the coulombic, voltage and energy efficiencies and discharge capacity over cycling for compound **2** and **4** can be found in the Supporting Information (Fig. S32).

3. Results and discussion

3.1. Synthesis of bipyridinium derivatives

A variety of 2,2′-bipyridinium salt derivatives (Fig. 1) were synthesized mainly by introduction of alkyl substituents at *N,N′* atoms. Typical synthetic route for preparation of quaternized bipyridines relies on the nucleophilic attack of the heteroaromatic compound over an

Table 1
Dihedral angles and C–C distances. Redox potential and other relevant parameters of RAM.

Molecule	Form	$E_{1/2}$ (V vs SHE) exp.	$E_{1/2}$ (V vs SHE) calc.	τ_1 (°)	r C_{ipso}-C'$_{ipso}$ bond (A)	D (cm^2/s)	k (cm/s)	λ (eV)	Solubility (M)
1	Ox	−0.39	−0.05	23.5	1.473	$7.24{\cdot}10^{-6}$	$1.54{\cdot}10^{-2}$	0.064	2.4
	Red			12.9	1.423				
2	Ox	−0.57	−0.27	54.0	1.482	$4.13{\cdot}10^{-6}$	$6.14{\cdot}10^{-3}$	0.143	2.8
	Red			35.5	1.434				
3	Ox	−0.67	−0.40	70.2	1.483	n.r	n.r	0.287	–
	Red			40.1	1.435				
4	Ox	−0.67	−0.41	53.4	1.479	$4.46{\cdot}10^{-6}$	$4.42{\cdot}10^{-3}$	0.132	2.2
	Red			35.1	1.434				
5	Ox	−0.70	−0.38	53.4	1.483	$5.59{\cdot}10^{-6}$	$1.58{\cdot}10^{-3}$	n.d	2.6
	Red			35.1	1.433				
6	Ox	−0.99	−1.01	53.5	1.484	n.r	n.r	n.r	–
	Red			37.7	1.441				
7	Ox	−0.37	0.27	54.1	1.482	$3.02{\cdot}10^{-6}$	$2.88{\cdot}10^{-2}$	n.d	–
	Red			38.5	1.445				
8	Ox	−0.12	0.11	53.6	1.487	n.s	n.s	n.s	<0.1
	Red			34.1	1.440				

t_1: N-C_{ipso}-C'$_{ipso}$-N (dihedral angle); $E_{1/2}$ vs SHE n.r: not reversible, n.d: not determined, n.s: not soluble.

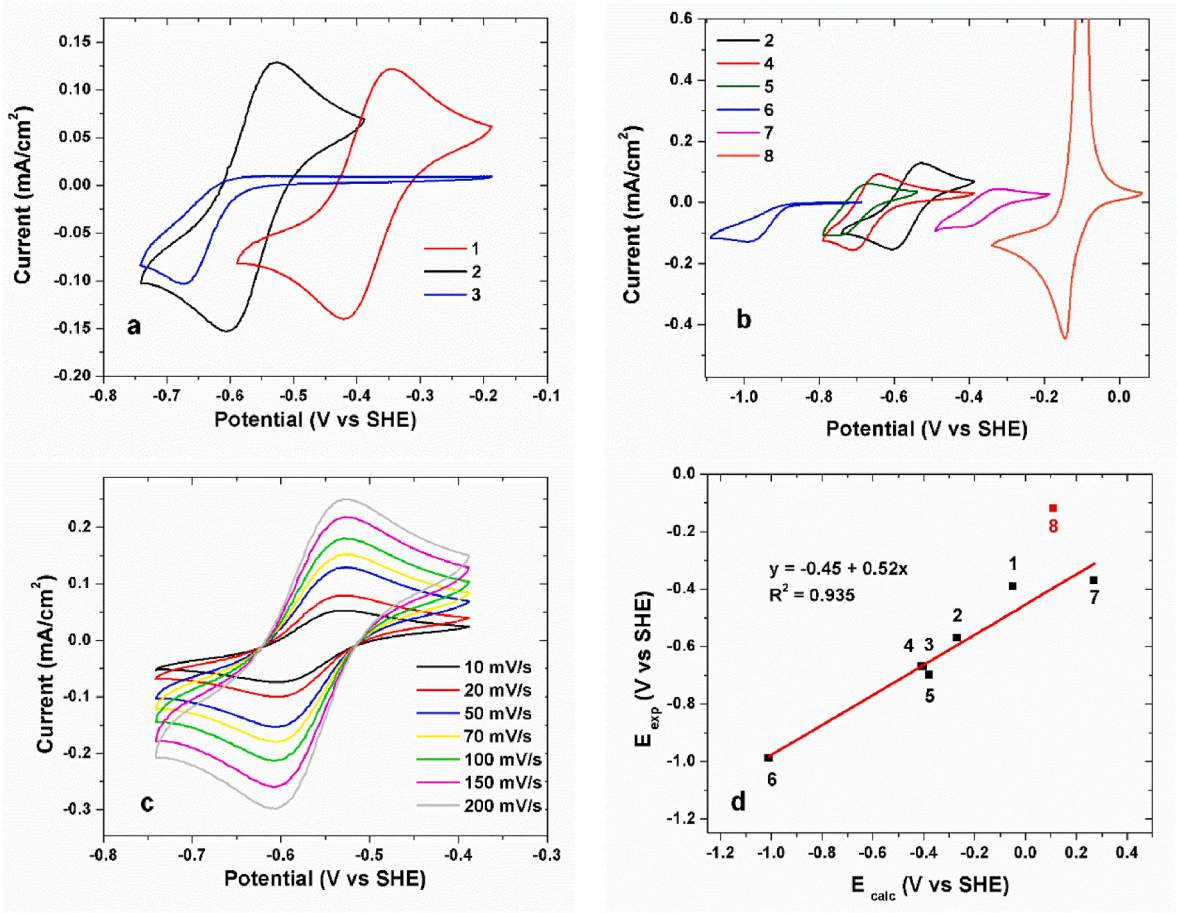

Fig. 2. Cyclic voltammogram at scan rate 50 mV/s of (a) **1**, **2** and **3**; (b) **2**, **4**, **5**, **6**, **7** and **8**. (c) Cyclic voltammograms of **2** at different scan rates (10–200 mV/s). (d) Comparison of calculated and experimental redox potentials. All the compounds were tested at 1 mM in 1 M NaCl solution at room temperature.

electrophile bearing a good leaving group, such as halogen, and the corresponding alkyl chain. This direct alkylation reaction is generally promoted by heat. Henceforth, two different highly efficient and sustainable protocols are proposed for obtaining the desired bipyridinium salts: (i) a solvent-free synthesis under standard reflux conditions, and (ii) an alternative microwave assisted coupling employing acetonitrile as solvent (for further information, see Scheme S1, S2 in the Supporting Information).

Therefore, a straightforward two-step synthetic route to desired 2,2′-bipyridinium salts (**1**–**8**) was envisioned. In a first step, the corresponding bipyridine reacts with a dibromoalkane leading to a tricyclic scaffold obtained by the formation of a third heterocyclic ring fused with original bipyridine molecule. The length of the linker between both nitrogen atoms is defined by the length of the alkyl chain in the dibromoalkane. Thus, dibromoethane, dibromopropane and dibromobutane substrates led to 6-, 7-, and 8-membered rings, depicted as **1**, **2** and **3** in Fig. 1. The quaternized bipyridine is initially obtained in the bromide salt form and subsequently transformed into the chloride salt in a final

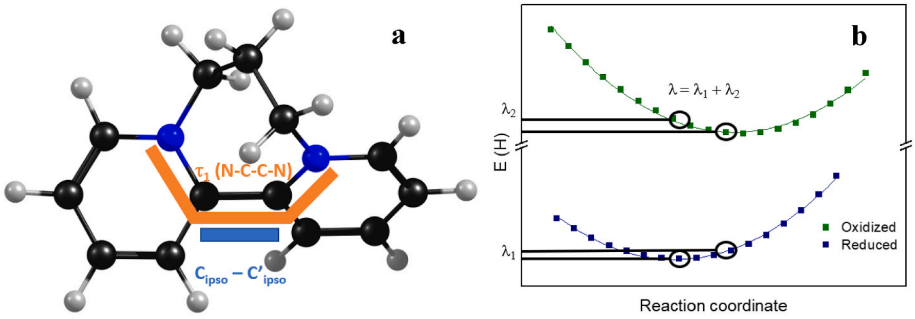

Fig. 3. Dihedral angle and C–C′ distance (**a**) and Schematic representation of Marcus parameters (**b**) for compound **4**.

quantitative anion-exchange step. Purity and chemical identity of the compounds was confirmed by ^{1}H NMR (see Supporting Information from Figs. S1–S16). Based on the ^{1}H and ^{13}C NMR spectra of the achieved compounds a purity >95% based on the NMR sensitivity can be assumed.

The versatility of the reaction was confirmed through the synthesis of a wide variety of compounds. Bipyridium salts with different size linkage (compounds **1**–**3**) could be isolated in good to excellent yields. Concerning compound **2** derivatives, the scope was successfully extended to bipyridines with different substitution patterns (*ortho*-, *meta*- and *para*-relative positions to nitrogen atom) including both electron donating (EDG) (*m*-Me **4**, *p*-Me **5** and *p*-MeO **6**), electron withdrawing groups (EWG) (p-COOH **7**) and extended aromatic systems (**8**) for evaluation of both structural and electronic effect on the electrochemical behaviour.

3.2. Physicochemical characterization

Initially, the electrochemical behaviour of synthesized derivatives from Fig. 1 was analysed. In this sense, the length of the alkyl linker is sufficient to alter the energy of both reduced and oxidized forms of bipyridinium salts in such a way that the change on the redox potential could be predicted by computational means. By applying the Hess's law, through the calculation of the energies of both gas and aqueous reduced and oxidized form (Scheme S3), the redox potentials of the different bipyridinium salts in solution were estimated (Table 1). Theoretical and experimental values, determined by cyclic voltammetry (CV) (Fig. 2a), show a similar trend when comparing the effects of the ring size (Table 1).

Interestingly, reversible reduction process of 7-membered ring derivative **2** is observed at a significantly low redox potential when compared to diquat **1** ($\Delta V = 0.18$ V). On the contrary, the redox process of 8-membered ring derivative (**3**) is completely irreversible and therefore, discarded as a candidate.

The degradation of the 2,2′-bipyridiniums salts has been linked to the relative disposition of pyridinium rings on the reduced state, being the proton-catalysed disproportionation one of the most common pathways [13,24]. Thus, calculations of the optimized geometries of these compounds were performed to determine key structural parameters which are summarized in Table 1 for both redox states. The dihedral angle formed by the two pyridyl rings and the length of the interring C_{ipso}--C'_{ipso} bond (Fig. 3a) are considered as benchmark for the π-delocalization over both aromatic rings. In all the cases, reduction leads to a significant decrease on the dihedral angle formed by the two pyridyl rings enabling the radical stabilization.

The reduced form of **1** presented a dihedral angle N–C–C′-N' (τ_1) (Fig. 3a) of 12.9°, in good accordance with the reported values [13], and an interring bond length of 1.423 Å. The obtained values were significantly lower than those calculated for **2** and **3** counterparts, which evidences a higher delocalization of the radical in compound **1** based on sp^2-hybridisation character of the interring bond. Even after a substantial decrease in the lowest-energy conformers of the reduced forms, compounds **2** and **3** could not lead to a more planar disposition due to geometrical restrictions, and therefore presented a longer interring bond and a higher dihedral angle (35–40°). The low redox potential of **2** and **3** might be explained by this higher dihedral angle and a poorer contribution of the second pyridinium ring to favour the reduction to the radical-cation intermediate.

The effect of the substituents on the bipyridyl rings was assessed in 7-membered ring derivatives (**4**–**8**) (Table 1). The core structure of **2** was the one selected due to the lower interring delocalization and expecting a more pronounced effect on stabilization that could be ascribed to the substituents as compared to **1**. Compound **2** stands as a candidate of interest with a lower redox potential and a non-planar structure that could somehow impede the stacking of bipyridines. Therefore, the challenge to overcome stability limitations of active materials of great interest based on critical properties as redox potential, solubility, geometry among other aspects is analysed in this work.

In case of the compounds with different ring size, the calculated values for the redox potential were comparable with those obtained experimentally (see Table 1 and Fig. 2). The change on electron density promoted by the EDGs or EWGs triggers the corresponding shift in the redox potential which follows the same trend predicted by computational means (Fig. 2b and d). Introduction of methyl group on *meta*- (**4**) or *para*- (**5**) positions to the pyridinic nitrogen decreases the redox potential on 0.1 V, while the methoxy moiety (**6**) further shifts the redox potential to lower values and turns the reduction into an irreversible process. On the contrary, the carboxylate substituent (**7**) increases the redox potential by 0.35 V, minimizing the practical interest of this compound as negolyte. The higher redox potential of biquinoline (**8**) was attributed to the extended aromatic structure and could not be accurately predicted by Hess's Law. Knowing that the Hess's Law uses the energies of the optimized geometries in aqueous and gas phases, the low solubility of **8** could lead to some deviations in the calculated redox potential (red dot in Fig. 2d). Moreover, a sharp peak was observed in the cyclic voltammogram of compound **8** suggesting the deposition/adsorption of material on the electrode surface. The non-linearity of the current with the square root of the scan rate suggests that redox species do not freely diffuse (Figure, S22). This phenomenon could be explained by the stronger interactions of the extended π-system within the glassy carbon electrode used in these measurements. The calculated redox potentials follow the same trend than the experimental ones. The differences between experimental and calculated values are in the order of the other reported works and could be ascribed to the different approximations [25].

Structural parameters do not significantly differ according to the substituents introduced, independently of their electronic nature (Fig. S28). However, *para*-substituted bipyridyl compounds (**5**–**7**) show slightly higher dihedral angle when substituent is other than methyl group. All in all, structural differences among 7-membered ring derivatives would not explain a different behaviour, which should be attributed then to the differences in electronic properties.

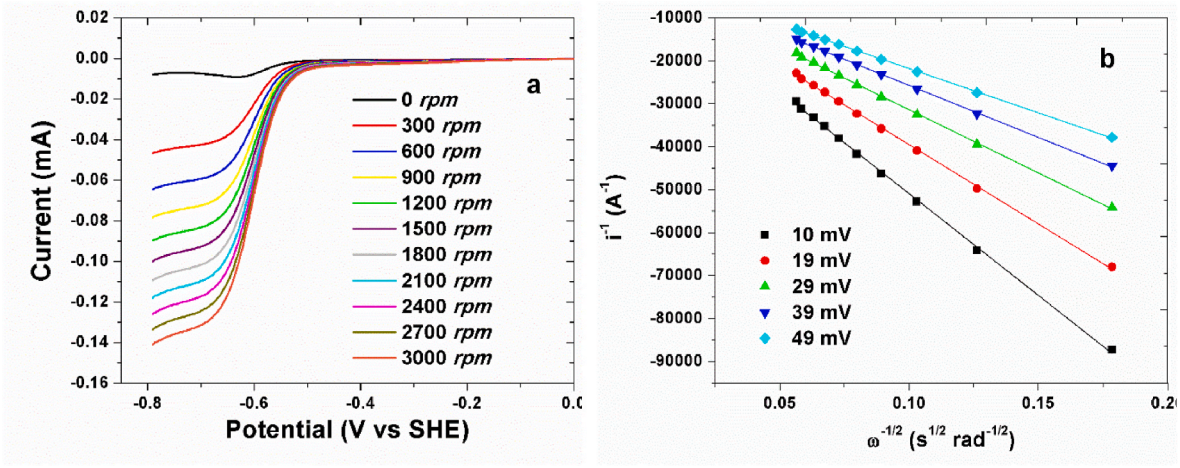

Fig. 4. Rotating-Disk-electrode (Glassy Carbon) experiments and Kinetic analysis of 1 mM **2** in 1 M NaCl: (a) LSV at 5 mV/s scan rate with rotation rates: 0, 300, 600, 900, 1200, 1500, 1800, 2100, 2400, 2700 and 3000 r.p.m.; (b) Kouyecký-Levich plot at different overpotentials.

Both alkylated derivatives (**4** and **5**) present remarkably lower C_{ipso}-C'_{ipso} distances in the reduced form. Higher C_{ipso}-C'_{ipso} distances were determined for compound **8**, which could be explained by the steric hindrance between the two quinoline moieties but also by the higher delocalization of the radical within the quinoline ring. Compound **6** presents the highest C_{ipso}-C'_{ipso} bond distance, which evidences a lower interring delocalization of the radical and is directly related to the irreversible redox process.

To gain further insight on the electron transfer reactions of these bipyridinium compounds, Marcus theory was applied considering no major structural changes between oxidized and reduced species. Thus, the potential energy surface versus the reaction coordinate (τ_1) of each redox species was considered for the calculation. In this case, the dihedral angle between pyridine rings was defined as reaction coordinate based on the change of this parameter according to the redox process (Fig. 3b) and the Marcus parameter values (λ) were calculated.

In parallel, the electron transfer rate (k) and diffusion coefficients (D) were determined experimentally from linear sweep voltammograms (LSV) using a rotating disk electrode (RDE) and calculated through the Koutecky-Levich and Levich equations, respectively (Fig. 4). Note that all the compounds present two redox processes (see Supporting Information Fig. S23) like it has been reported previously for viologen (and 2,2′-bipyridine) derivatives but just the first represent a fast reversible process [13,24]. For this reason, just the kinetic constants and diffusion coefficients of the first electron ($n = 1$) for compounds that are reversible has been studied. The Marcus parameter can be correlated with the determined kinetic constants as collected in Table 1, where a high value for this parameter corresponds to a slow kinetic redox process. Thus, the electron-transfer rate constants obtained were $1.54{\cdot}10^{-2}$ and $6.14{\cdot}10^{-3}$ cm/s for compounds **1** and **2,** respectively. In case of compound **3**, the obtained value was significantly higher than the one obtained for compounds **1** and **2**, suggesting a less favourable reduction process and a higher inversion barrier between oxidized and reduced forms. On the other hand, the substituents on the aromatic ring did not lead to significant changes on the reaction kinetics. Based on the small structural differences among 7-membered ring derivatives, as evidenced by the dihedral angle variations and C_{ipso}-C'_{ipso} values, Marcus parameter would not be appropriate to compare these compounds (**2** = 0.143 eV vs **4** = 0.132 eV). The faster kinetics experimentally observed for compound **7** are ascribed to the electron withdrawing character of carboxylate substituent and cannot be predicted by Marcus theory.

The water solubility is an important property considering the potential application of these materials as negolytes in RFB. The molar water solubility of 2,2′-bipyridynium compounds was measured by UV/Vis spectroscopy (Table 1). The higher solubility of the 7-membered ring **2** (2.8 M) when compared to diquat, **1** (2.4 M), may be attributed to the lower planarity and higher polarity conferred by the longer alkyl linker bridging nitrogen atoms. By contrast, the solubility of substituted

a

Molecules	Normalized Degree of delocalization
1	1.02
2	1
3	0.84
4	73.49
5	11.54
6	0.64
7	19.10
8	774.75

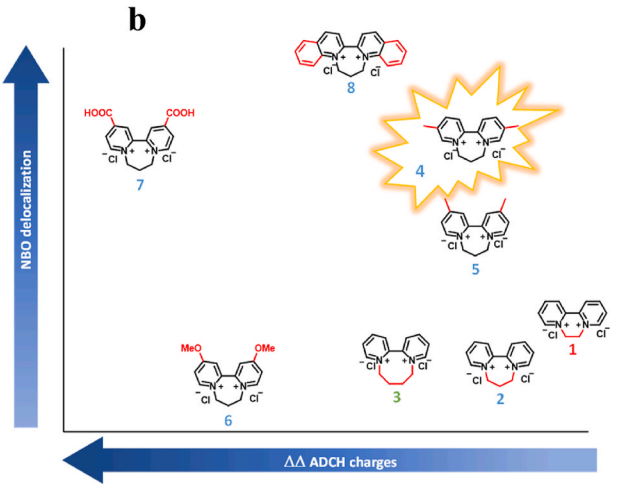

Fig. 5. (a) Sum of the delocalization interactions between the NBO. (b) Illustrative figure evaluating the contribution of the NBO delocalization and the ADCH charge distribution.

bipyridinium salts **4**, **5** and **8** confirmed the relevance of both the nature of the substituents and the disposition of them in the core structure. Thus, methyl substituents in *meta*- and *para*-positions have opposite effect on solubility. Worth noting, *para*-substituted bipyridinium compound showed higher solubility, up to 2.6 M. Nevertheless, the substitution of pyridinic rings by more delocalized quinolinic rings led to a dramatic drop on water solubility (<0.1 M). The latter is in good agreement with the hypothesis of material deposition on electrode surface during cyclic voltammetry experiment for compound **8**. The more hydrophobic character of compound **8** and the potentially stronger π-π interactions shall explain the lower water solubility.

3.3. DFT calculation

Computational tools can accurately predict the electrochemical properties of the compounds (e.g. E_{red}) and stablish clear trends linked to structural and electronic modifications on the active materials. However, the stability of these materials requires deeper analysis, especially of charged species. Reduction of bipyridinium rings results in cation-radical species which could undergo side reactions. These species are stabilized by the radical delocalization between the two aromatic rings [8]. The analysis of the Natural Bond Orbitals (NBO) and the ADCH charges was proposed for better understanding of the interring radical delocalization and the atomic charge distribution.

Based on the analysis of the Natural Bond Orbitals of the reduced species, a comparison of the electronic delocalization for the different bipyridinium derivatives was performed (Fig. 5, Table S2). As it can be seen in Fig. 5, derivatives **1**, **2** and **3** show similar electronic delocalization, being higher as shorter the bridge is (**1** ≈ **2** > **3**). Thus, the higher delocalization forecasted by NBO analysis fits with the previously calculated structural parameters, as the dihedral angle and the interring bond distance. When focusing on the role of substituents, it could be observed that substituents which do not allow delocalization present lower interactions, for example strong EDG in **6** inhibit the delocalization between the two aromatic rings. The expansion of aromaticity (compound **8**) significantly enhances the delocalization because of the increased number of interactions. In principle, this higher level of interactions should correspond to a more stable reduced form. However, the mismatch between theoretical and experimental outcome may be explained by the low water solubility of compound **8.** The addition of a methyl group also enhances the delocalization between the two aromatics moieties (**4** and **5**). The methyl group acts as a weak donor substituent enhancing the NBO interactions between the two aromatic rings. When the focus is put on the *para* position, it could be observed that higher electron withdrawing character of the substituent enhances the delocalization between the aromatic rings (compound **7**).

The influence of the interring delocalization on the stability of the reduced radical has been reinforced by the study of the charge distribution which show how the electron in the reduced form has been allocated. The difference between the change in each carbon of the aromatic ring (*ortho-*, *meta-* and *para*-relative positions to the nitrogen of the pyridine) when comparing oxidized and reduced forms define the symmetric or nonsymmetric distribution between both aromatic rings. By comparing this distribution between two aromatic rings, it can be determined if the charge has been allocated in both aromatic rings or preferentially in one of them, making both rings different (Table S3) [8]. In this study different population analysis has been compared considering their strengths and weaknesses: Mulliken [26], Hirshfeld [27] and Atom Dipole Correction Hirshfeld (ADCH) [28]. While Mulliken analysis is a well extended method it is not ideal for practical applications due to the poor reproducibility of observable properties such as molecular dipole moment, a very high basis dependence and occasionally meaningless results. On the contrary, Hirshfeld analysis leads to qualitatively consistent results with the general chemical concepts, and it is insensitive to the size of the wavefunction, and the applicability of the Hirshfeld population is not constrained by the type of wavefunction. The con of this method is that the charges are always too small and the poor reproducibility of observable quantities because the Hirshfeld population completely ignores atomic dipole moments. In this sense, the Atomic Dipole Corrected Hirshfeld (ADCH) analysis takes into account the atomic dipole moment and the charges achieved are significantly higher. The three analysed methods lead to similar trends when comparing bipyridinium derivatives, see Table S3 and Supporting Information for more details. The ADCH method was selected. If the bipyridinium derivative presents high delocalization, the difference in the charge distribution should be low. For example, compounds **1** and **2** show almost negligible difference between the charge distribution for both aromatic rings. The compound **3** shows higher differences, which is aligned with previous predictions based on the higher dihedral angle and resultant lower delocalization. When turning into the study of the effect of the substituents, similarly to what has been observed in the NBO analysis, the introduction of strong EDG or EWG has a detrimental effect on the interactions or interring delocalization as evidenced by the significant differences between aromatic rings in terms of charge allocation determined for compounds **6** and **7**. Compound **8**, which according to NBO analysis show an increase number of interring interactions, presents a lower interring delocalization than the non-substituted pyridinium homologue. A preferential delocalization within the quinoline ring is therefore expected for compound **8**, which according to delocalization predicted in the NBO and charge analysis could be a highly stable active material. However, it is discarded based on its poor solubility. Finally, the methyl group **4** and **5** show quite similar charge distribution between the two pyridine rings. Again, mild EDG seem to somehow promote further interactions between rings and charge delocalization. Thus, high stability for the cation radical reduced species is foreseen for those bipyridinium derivatives.

Charge analysis have been proposed as a powerful tool that combined with NBO and structural analysis, provide deeper understanding on the stability of these compounds. Note that Fig. 5 shows, in a representative way, the contribution of NBO delocalization and the ADCH (most chemically meaningful of the three studied methods) charge distribution to the stability of the bipyridinium derivatives and serves as a plausible guidance in the selection of a good candidate for a potential RFB. Thereby, by considering both contributions, bipyridine derivatives with high delocalization are expected to render more stable electrolytes due to the high stabilization of the cation radical.

Encouraged by the computational studies, compound **4** was selected for the preparation and testing of electrolytes for AORFB. Therefore, based on the given theoretical predictions, single cell tests were addressed to corroborate the stability of its reduced form.

3.4. Flow cell tests

Bures et al. reported the single cell test using **1** as negolyte in a bulk-electrolysis where the stability of the negolyte was studied [29]. Taking this reference as starting point and matching their results with our predicting model we expect that **1** and **2** show similar results in terms of stability as can be interpreted from Fig. 5. Besides, to corroborate the predicted stability of **4** over **2** by DFT analysis, both materials were integrated in a single cell set-up subjected to repetitive charge-discharge cycles employing TEMPOL as reference posolyte material. Both tests were performed under comparable operating conditions, by using the same carbon felts as electrodes, membrane, electrolyte concentration and charge-discharge conditions (see the SI for detailed information). The battery was charged and discharged at constant current and constant voltage ensuring that the negolyte reaches the desired SoC minimizing effect of overpotential. This methodology was proposed with the aim of comparing the stability of electrolytes which present differences in the electrochemical properties, such as redox potential, kinetic constant, and diffusion coefficient. Equally, to avoid the influence of the posolyte, an excess of TEMPOL was used.

On this basis, the capacity decay is mainly ascribed to side reactions.

Table 2
Results of the single cell tests performed with **2** and **4** as respective negolytes. Interval between the first and last efficiencies, capacity, capacity utilization and capacity decay.

(RAM)	CE (%)	VE (%)	EE (%)	$Q_{discharge}$ (mAh)	CU (%)	dQdis/dn (mAh)	d%Qdis/dn (%)
2	97.8–100.2	57.7–23.7	56.7–23.4	32.3–17.7	80.4–44.0	0.285	0.71
4	93.6–100.4	63.6–42.0	63.6–41.5	33.4–4.7	83.1–11,6	0.141	0.35

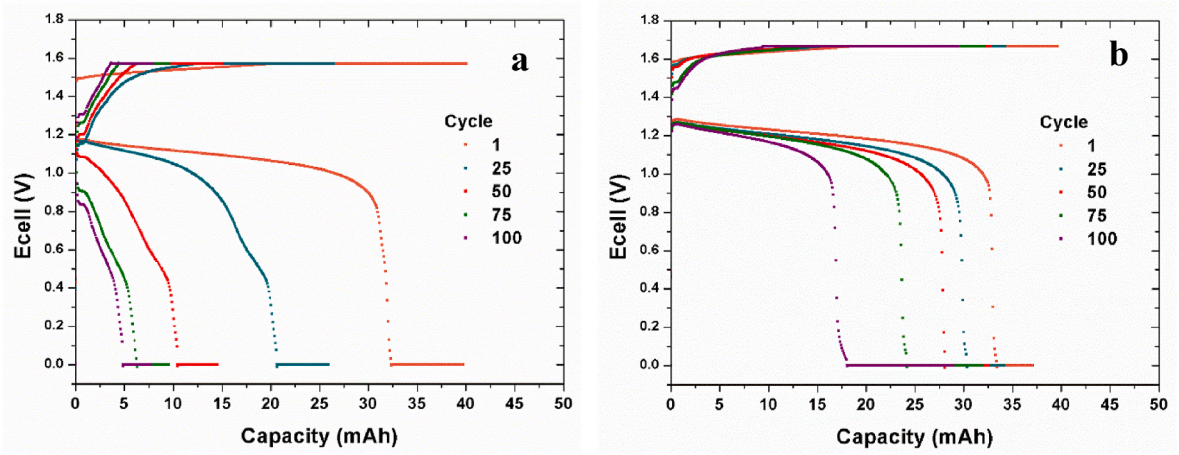

Fig. 6. (a): Single cell results using 0.1 M of **2** as negolyte vs 0.15 M of TEMPOL as posolyte, 100 cycles at room temperature, (b) Single cell results using 0.1 M of **4** as negolyte vs 0.15 M of TEMPOL as posolyte, 100 cycles at room temperature.

As it can be seen in Table 2 and Fig. 6, the electrolyte based on compound **2** presents higher capacity fade compared to compound **4**. When solely comparing the galvanostatic step, capacity losses are reduced to half for the battery employing compound **4** (0.285 mAh/cycle, 0.71%/cycle vs 0.141mAh/cycle, 0.35%/cycle, respectively). The difference is even more noticeable when the potentiometric step is considered (0.301 mAh/cycle, 0.75%/cycles vs 0.065 mAh/cycle 0.16%/cycle, respectively). Thus, the negolyte based on compound **4** can deliver capacities close to 92.2–72.0% of the theoretical value, which could be taken as indicator of the state of health of the active material. On the contrary, negolyte based on compound **2** initially delivered 98.5% of the theoretical capacity, but after 100 cycles just 20.8% of the theoretical capacity was achieved, indicating that active material cannot longer store energy even when negative cell polarization effect is avoided. Also, despite the differences in the experiment performed by Bures et al., we can observe clearly that **1** and **2** show practically same capacity decay which correlates with the presented predicting model. Indeed, the charge-discharge profiles (Fig. 6) denote significant changes in the electrochemical behavior of compound **2** over cycling. After few cycles a new plateau can be inferred in the range of 0.4–0.6 V, this is certainly related to changes in the behaviour of the active material which potentially could form aggregates or directly undergo side reaction. This phenomenon together with the observed capacity decay emphasizes the undesired electrolyte transformation during cycling. The evaluation of charged and cycled-aged electrolytes based on compound **2** allowed to confirm the formation of side products as the protonation product (**2b**), which could account for the observed fast capacity decay (see Supporting Information) [13]. Capacity falls far below 30% while cell polarization increases substantially. On the contrary, *meta* substituted derivative, **4**, despite the observed capacity decay, outperforms compound **2** in terms of cycling stability while no significant change is observed in the profile. Initially, both compounds show similar results in terms of coulombic, voltage and energy efficiency, however the capacity decay observed in the following cycles correlates with a poor battery performance (Fig. S33). These results are in good agreement with the results predicted by the DFT analysis in the previous section. Therefore, it proves the importance of putting efforts on the understanding of the electrolyte properties and the requirements of the molecular structure to increase their stability at both charged states.

4. Conclusions

The stability of organic compounds for application in RFB is still to be understood and confirmed for the deployment of AORFB. In this work, an expansion of the DFT calculation in RFB has been proposed as a predictive tool for the stability of those batteries. The proposed methodology has been applied to a wide diversity of 2,2′-bipyridine derivatives both in terms of structure and the electronic density. 1,1′-1,3-propylene-2,2′-bipyridinium salts can be easily reached through a straightforward synthesis and present outstanding properties for application as negolyte, high water solubility (up to 2.8 M) and low redox potentials (ca. −0.7 V vs SHE). Those bipyridinium derivatives have demonstrated viable AORFB performance when integrated in a flow cell. DFT calculations on structural parameters, such as the dihedral angle and the C_{ipso}-C'_{ipso} distance on the bipyridines, were applied to foresee redox properties (kinetic constant, redox potential) of molecules with remarkable structural differences, compounds **1**–**3**. Given the similar geometry of 7-membered ring derivatives (**4**–**8**), a novel strategy based on NBO and ADCH charge analysis was proposed to study the influence of different electronic nature substituents on the stability of the active materials. For the first time, NBO analysis has been used to understand the delocalization of the radical generated in the reduction of these derivatives. Interestingly, the analysis of the distribution of the ADCH charges in the oxidized and reduced forms between two aromatic rings has reinforced the study. Thereby, this complementary study served to identify compound **4** among evaluated derivatives as the most stable material to be applied in AORFB considering the delocalization and charge distribution. The predictive capability of this methodology was corroborated in flow cell studies by the higher capacity retention observed for compound **4** based negolyte. The poor stability of reference compound **2** could be confirmed based on detected side products that lead to irreversible capacity losses. The excellent theoretical-experimental correlation unveils the powerful predicting ability of DFT calculations for Redox Flow Batteries and opens a new avenue for

the development of a new generation of organic redox active materials through DFT-aided stability modulation strategies.

CRediT authorship contribution statement

Juan Asenjo-Pascual: Conceptualization, Methodology, Formal analysis, Validation, Investigation, Writing – original draft, Writing – review & editing, and, Visualization. **Ivan Salmeron-Sanchez:** Conceptualization, Methodology, Validation, Investigation, Writing – review & editing, and, Visualization. **Pablo Mauleón:** Conceptualization, Writing – review & editing, and, Funding acquisition. **Maddalen Agirre:** Methodology, Resources, and, Writing – review & editing. **Ana Catarina Lopes:** Methodology, Resources. **Oihane Zugazua:** Methodology, Resources. **Eduardo Sánchez-Díez:** Conceptualization, Methodology, Resources, Writing – review & editing, and, Funding acquisition. **Juan Ramón Avilés-Moreno:** Conceptualization, Methodology, Validation, Writing – review & editing, Supervision, and, Funding acquisition. **Pilar Ocón:** Conceptualization, Methodology, Validation, Resources, Writing – review & editing, Supervision, and, Funding acquisition, All authors gave approval to the final version of the manuscript.

Declaration of competing interest

The authors declare the following financial interests/personal relationships which may be considered as potential competing interests: Pilar Ocon Esteban reports financial support was provided by European Union. Eduardo Sanchez Diez reports financial support was provided by European Union. Juan Ramon Aviles Moreno reports financial support was provided by European Union. Pablo Mauleon reports financial support was provided by European Union.

Data availability

No data was used for the research described in the article.

Acknowledgements

This work has been funded by the European Union under the HIGREEW project, Affordable High-performance Green Redox Flow batteries (Grant agreement no. 875613). H2020: LC-BAT-4-2019. A.C. Lopes acknowledges the Ramon y Cajal (RYC2021-032277-I) research fellowship, the financial support from Ministerio de Ciencia e Innovación / AEI /10.13039/501100011033 and from European Union NextGenerationEU/PRTR. We also thank the CCC-UAM (Graforr project) for allocation of computer time.

Appendix A. Supplementary data

Supplementary data to this article can be found online at https://doi.org/10.1016/j.jpowsour.2023.232817.

References

[1] (a) M.S. Dreselhaus, I.L. Thomas, Alternative energy technologies, Nature 414 (2001) 332–337;
(b) A. Sternberg, A. Bardow, Power-to-what?-Environmental assessment of energy storage systems, Energy Environ. Sci. 8 (2015) 389–400;
(c) Z.G. Yang, J.L. Zhang, M.C.W. Kintner-Meyer, X.H. Lu, D. Choi, J.P. Lemmon, J. Liu, Electrochemical energy storage for green grid, Chem. Rev. 111 (2011) 3577–3613.

[2] (a) O. Krishan, S. Suhag, An updated review of energy storage systems: classification and applications in distributed generation power systems incorporating renewable energy resources, Int. J. Energy Res. 43 (2019) 6171–6210;
(b) A.G. Olabi, C. Onumaegbu, T. Wilberforce, M. Ramadan, M.A. Abdelkareem, A.H.A. Alami, Critical review of energy storage systems, Energy 214 (2021) 118987–119009.

[3] SET plan action 7 of the SET plan on "batteries for e-mobility and stationary storage. https://setis.ec.europa.eu/system/files/2021-05/action7_declaration_of_intent_0.pdf.

[4] (a) J. Noack, N. Roznyatovskaya, T. Herr, P. Fischer, The chemistry of redox-flow batteries, Angew. Chem., Int. Ed. 54 (2015) 9776–9809;
(b) G.L. Soloveichik, Flow batteries: current status and trends, Chem. Rev. 115 (2015) 11533–11558;
(c) M. Skyllas-Kazacos, M.H. Chakrabarti, S.A. Hajimolana, F.S. Mjalli, M. Saleem, Progress in flow battery research and development, J. Electrochem. Soc. 158 (2011) R55–R79;
(d) A.Z. Weber, M.M. Mench, J.P. Meyers, P.N. Ross, J.T. Gostick, Q. Liu, Redox flow batteries: a review, J. Appl. Electrochem. 41 (2011) 1137–1164.

[5] (a) A. Mousa, M. Skyllas-Kazacos, Effect of additives on the low-temperature stability of vanadium redox flow battery negative half-cell electrolyte, Chemelectrochem 2 (2015) 1742–1751;
(b) S. Roe, C. Menictas, M. Skyllas-Kazacos, A high energy density vanadium redox flow battery with 3 M vanadium electrolyte, J. Electrochem. Soc. 163 (2016) A5023–A5028;
(c) M. Skyllas-Kazacos, L. Cao, M. Kazacos, N. Kausar, A. Mousa, Vanadium electrolyte studies for the vanadium redox battery—a review, ChemSusChem 9 (2016) 1521–1543;
(d) . https://www.vanitec.org/vanadium-redox-flow-battery-vrfb-companies.

[6] (a) V. Singh, S. Kim, J. Kang, H.R. Byon, Aqueous organic redox flow batteries, Nano Res. 12 (2019) 1988–2001;
(b) J. Winsberg, T. Hagemann, T. Janoschka, M.D. Hager, U.S. Schubert, Redox-flow batterires: from metals to organic redox-active materials, Angew. Chem., Int. Ed. 56 (2017) 686–711;
(c) Y. Dind, C. Zhang, L. Zhang, Y. Zhou, G. Yu, Molecular engineering of organic electroactive materials for redox flow batteries, Chem. Soc. Rev. 47 (2018) 69–103.

[7] (a) F. Zhong, M. Yang, M. Ding, C. Jia, Organic electroactive molecule-based electrolytes for redox flow batteries: status and challenges of molecular design, Front. Chem. 8 (2020) 451–464;
(b) D.G. Kwani, Y. Ji, M.J. Aziz, Electrolyte lifetime in aqueous organic redox flow batteries: a critical review, Chem. Rev. 120 (2020) 6467–6489.

[8] J.D. Griffin, A.R. Pancoast, M.S. Sigman, Interrogation of 2,2′-bipyrimidines as low-potential two-electron electrolytes, J. Am. Chem. Soc. 143 (2021) 992–1004.

[9] (a) S. Jin, E.M. Fell, L. Vina-Lopez, Y. Jing, P.W. Michalak, R.G. Gordon, M.J. Aziz, Near neutral pH redox flow battery with low permeability and long-lifetime phosphonated viologen active species, Adv. Energy Mater. 10 (2020) 2000100–2000110;
(b) C. DeBruler, B. Hu, J. Moss, J. Luo, T.L. Liu, A sulfonate-functionalized viologen enabling neutral cation exchange, aqueous organic redox flow batteries toward renewable energy storage, ACS Energy Lett. 3 (2018) 663–668;
(c) J. Luo, B. Hu, C. DeBruler, T.L. Liu, A π-conjugation extended viologen as a two-electron storage anolyte for total organic aqueous redox flow batteries, Angew. Chem. Int. Ed. 57 (2018) 231–235;
(d) C. DeBruler, B. Hu, J. Moss, X. Liu, J. Luo, Y. Sun, T.L. Liu, Designer two-electron storage viologen anolyte materials for neutral aqueous organic redox flow batteries, Chem 3 (2017) 961–978;
(e) J. Luo, B. Hu, C. Debruler, Y. Bi, Y. Zhao, B. Yuan, M. Hu, W. Wu, T.L. Liu, Unprecedented capacity and stability of ammonium ferrocyanide catholyte in pH neutral aqueous redox flow batteries, Joule 3 (2019) 149–163;
(f) M. Hu, W. Wu, J. Luo, T.L. Liu, Desymmetrization of viologen anolytes empowering energy dense, ultra stable flow batteries toward long-duration energy storage, Adv. Energy Mater. 12 (2022) 2202085–2202093;
(g) H. Li, H. Fan, B. Hu, L. Hu, G. Chang, J. Song, Spatial structure regulation: a rod-shaped viologen enables long lifetime in aqueous redox flow batteries, Angew. Chem. Int. Ed. 60 (2021) 26971–26977;
(h) M. Gao, M. Salla, Y. Song, Q. Wang, High-power near-neutral aqueous all organic redox flow battery enabled with a pair of anionic redox species, Angew. Chem. Int. Ed. 61 (2022), e2022082.

[10] E.S. Beh, D.D. Porcellinis, R.L. Gracia, K.T. Xia, R.G. Gordon, M.J. Aziz, A neutral pH aqueous organic–organometallic redox flow battery with extremely high capacity retention, ACS Energy Lett. 2 (2017) 639–644.

[11] (a) T. Ayabe, B. Chan, T. Sagara, Fluorination effect on electrochemistry of dibutyl viologen in aqueous solution, J. Electroanal. Chem. 856 (2020) 113691–113697;
(b) C. Chen, S. Zhang, Y. Zhu, Y. Qian, Z. Niu, J. Ye, Y. Zhao, X. Zhang, Pyridyl group design in viologens for anolyte materials in organic redox flow batteries, RSC Adv. 8 (2018) 18762–18770;
(c) S.C. Dorman, R.A. O'Brien, A.T. Lewis, E.A. Salter, A. Wierzbicki, P.W. Hixon, R.E. Sykora, A. Mirjafari, J.H. Davis Jr., A new building block for electroactive organic materials? Synthesis, cyclic voltammetry, single crystal X-ray structure, and DFT treatment of a unique boron-based viologen, Chem. Commun. 47 (2011) 9072–9074.

[12] R.J. Mortimer, Organic electrochromic materials, Electrochim. Acta 44 (1999) 2971–2981.

[13] J. Huang, Z. Yang, V. Murugesan, E. Walter, A. Hollas, B. Pan, R.S. Assary, I. A. Shkrob, X. Wei, Z. Zhang, Spatially constrained organic diquat anolyte for stable aqueous flow batteries, ACS Energy Lett. 3 (2018) 2533–2538.

[14] (a) M. Pan, L. Gao, J. Liang, P. Zhang, S. Lu, Y. Lu, J. Ma, Z. Jin, Reversible redox chemistry in pyrrolidinium-based TEMPO radical and extended viologen for high-voltage and long-life aqueous redox flow batteries, Adv. Energy Mater. 12 (2022) 2103478–2103486;
(b) H. Fan, W. Wu, M. Ravivarma, H. Li, B. Hu, J. Lei, Y. Feng, X. Sun, J. Song, T. L. Liu, Mitigating ring-opening to develop stable TEMPO catholytes for pH-neutral all-organic redox flow batteries, Adv. Funct. Mater. 32 (2022) 2203032–2203041;

(c) H. Fan, H. Li, M. Ravivarma, Y. Feng, J. Song, Conjugate-driven electron density delocalization of piperidine nitroxyl radical for stable aqueous zinc hybrid flow batteries, Angew. Chem. Int. Ed. 61 (2022), e2021159.

[15] (a) B. Hu, M. Hu, J. Luo, T.L. Liu, A stable, low permeable TEMPO catholyte for aqueous total organic redox flow batteries, Adv. Energy Mater. 12 (2022) 2102577–2102582;
(b) X.-L. Lv, P. Sullivan, H.-C. Fu, X. Hu, H. Liu, S. Jin, W. Li, D. Feng, Dextrosil-viologen: a robust and sustainable anolyte for aqueous organic redox flow batteries, ACS Energy Lett. 7 (2022) 2428–2434;
(c) M. Huang, S. Hu, X. Yuan, J. Huang, W. Li, Z. Xiang, Z. Fu, Z. Liang, Five-membered-heterocycle bridged viologen with high voltage and superior stability for flow battery, Adv. Funct. Mater. 32 (2022) 2111744–2111751.

[16] M.A. Goulet, M.J. Aziz, Flow battery molecular reactant stability determined by symmetric cell cycling methods, J. Electrochem. Soc. 165 (2018) A1466–A1477.

[17] M.J. Frisch, G.W. Trucks, H.B. Schegel, G.E. Scuseria, M.A. Robb, J.R. Cheeseman, G. Scalmani, V. Barone, G.A. Petersson, H. Nakatsuji, X. Li, M. Caricato, A. V. Marenich, J. Bloino, B.G. Janesko, R. Gomperts, B. Mennucci, H.P. Hratchian, J. V. Ortiz, A.F. Izmaylov, L. Sonnenberg, D. Williams-Young, F. Ding, F. Lipparini, F. Egidi, J. Goings, B. Peng, A. Petrone, T. Henderson, D. Ranasinghe, V. G. Zakrewski, J. Gao, N. Rega, G. Zheng, W. Liang, M. Hada, M. Ehara, K. Toyota, R. Fukuda, J. Hasegawa, M. Ishida, T. Nakajima, Y. Honda, O. Kitao, H. Nakai, T. Vreven, K. Thorssell, J.A. Montgomery Jr., J.E. Peralta, F. Ogliaro, M. J. Bearpark, J.J. Heyd, E.N. Brothers, K.N. Kudin, V.N. Staroverov, T.A. Keith, R. Kobayashi, J. Normand, K. Raghavachari, A.P. Rendell, J.C. Burant, S.S. Iyengar, J. Tomasi, M. Cossi, J.M. Millam, M. Klene, C. Adamo, R. Cammi, J.W. Ochterski, R.L. Martin, K. Morokuma, O. Farkas, J.B. Foresman, D.J. Fox, Gaussian 16, Revision C. 01, Gaussian Inc., Wallingford CT, 2016.

[18] G.A. Petersson, A. Bennett, T.G. Tensfeldt, M.A. Al-Laham, W.A. Shirley, J. Mantzaris, A complete basis set model chemistry I. The total energies of closed-shell atoms and hydrides of the first-row atoms, J. Chem. Phys. 89 (1988) 2193–2218.

[19] a) A.D. Becke, Density-functional exchange-energy approximation with correct asymptotic behavior, Phys. Rev. A 38 (1988) 3098–3100;
b) C. Lee, W. Yang, R.G. Parr, Development of the colle-salvetti correlation-energy formula into a functional of the electron density, Chem. Phys. B 37 (1988) 785–789;
c) A.D. Becke, Density functional thermochemistry III. The role of exact exchange, J. Chem. Phys. 98 (1993) 5648–5652.

[20] a) Y. Zhao, D.G. Truhlar, Applications and validations of the Minnesota density functionals, Chem. Phys. Lett. 502 (2011) 1–13;
b) N. Mardirossian, J.A. Parkhill, M. Head-Gordon, Benchmark results for empirical post-GGA functionals: difficult exchange problems and independent tests, Phys. Chem. Chem. Phys. 13 (2011) 19325–19337.

[21] S. Grimme, S. Ehrlich, L. Goerigk, Effect of the damping function in dispersion corrected density functional theory, J. Comput. Chem. 32 (2011) 1456–1465.

[22] S.N. Steinmann, C. Piemontesi, A. Delachat, C. Corminboeuf, Why are the interaction energies of charge-transfer complexes challenging for DFT? J. Chem. Theor. Comput. 8 (2012) 1629–1640.

[23] J. Tomasi, B. Mennucci, R. Cammi, Quantum mechanical continuum solvation models, Chem. Rev. 105 (2005) 2999–3093.

[24] (a) M. Heyrovsky, The electroreduction of methyl viologen, J. Chem. Soc., Chem. Commun. 24 (1987) 1856–1857;
(b) T. Liu, X. Wei, Z. Nie, V. Sprenkle, W. Wang, A total organic aqueous redox flow battery employing a low cost and sustainable methyl viologen anolyte and 4-HO-TEMPO catholyte, Adv. Energy Mater. 6 (2016), 1501449-150-1457;
(c) Y. Lv, Y. Liu, T. Feng, J. Zhang, S. Lu, H. Wang, Y. Xiang, Structure reorganization-controlled electron transfer of bipyridine derivatives as organic redox couples, J. Mater. Chem. A. 7 (2019) 27016–27022.

[25] (a) S. Ghule, S.R. Dash, S. Bagchi, K. Joshi, K. Vanka, Predicting the redox potentials of phenazine derivatives using DFT-assisted machine learning, ACS Omega 7 (2022) 11742–11755;
(b) J.F. Kucahryson, L. Cheng, S.O. Tung, L.A. Curtiss, L.T. Thompson, Predicting the potentials, solubilities and stabilities of metal-acetylacetonates for non-aqueous redox flow batteries using density functional theory calculations, J. Mater. Chem. 5 (2017) 13700–13709.

[26] R.S. Mulliken, Electronic population analysis on LCAO–MO molecular wave functions. II. Overlap populations, bond orders, and covalent bond energies, J. Chem. Phys. 23 (1955) 1841–1846.

[27] F.L. Hirshfeld, Bonded-atom fragments for describing molecular charge densities, Theor. Chim. Acta 44 (1977) 129–138.

[28] T. Lu, F. Chen, Atomic dipole moment corrected Hirshfeld population method, J. Theor. Comput. Chem. 11 (2012) 163–183.

[29] Z. Buresova, M. Klikar, P. Mazur, M. Mikesova, J. Kvícala, T. Bystron, F. Bures, Redox property tuning in bipyridinium salts, Front. Chem. 8 (2020) 631477–631486.